UCLA
COMPUTATIONAL AND APPLIED MATHEMATICS

Robust Difference Approximations of Stiff Inviscid Detonation Waves

Bjorn Engquist
Bjorn Sjogreen

March 1991

CAM Report 91-03

Department of Mathematics
University of California, Los Angeles
Los Angeles, CA. 90024-1555

UCLA
COMPUTATIONAL AND APPLIED MATHEMATICS

Robust Difference Approximations of Stiff Inviscid Detonation Waves

Bjorn Engquist
Bjorn Sjogreen

March 1991

CAM Report 91-03

Department of Mathematics
University of California, Los Angeles
Los Angeles, CA. 90024-1555

ROBUST DIFFERENCE APPROXIMATIONS OF STIFF INVISCID DETONATION WAVES

Bjorn Engquist[1] and Björn Sjögreen[2]

Abstract. Inviscid compressible fluid with a one step irreversible chemical reaction is approximated by finite difference methods. We compute detonation wave solutions using new higher order TVD/ENO numerical methods for the convective part of the equations, and we show how the source term can be incorporated into the Runge-Kutta time marching scheme. In this type of combustion problem stiff source terms can lead to unphysical wave speeds. A remedy for this behavior is developed and implemented. We present results in one and two space dimensions, showing that the stiffness problem can be avoided by using this new method. We also give numerical results regarding the oscillatory behavior of the pressure peak in the one dimensional ZND detonation wave.

Key words. detonation, shock capturing difference method

AMS(MOS) subject classifications. 65P05, 76L05, 80A32

1. Introduction. We consider the equations

$$\begin{pmatrix} \rho \\ m \\ n \\ e \\ \rho z \end{pmatrix}_t + \begin{pmatrix} m \\ m^2/\rho + p \\ mn/\rho \\ m(e+p)/\rho \\ mz \end{pmatrix}_x + \begin{pmatrix} n \\ mn/\rho \\ n^2/\rho + p \\ n(e+p)/\rho \\ nz \end{pmatrix}_y = \begin{pmatrix} 0 \\ 0 \\ 0 \\ 0 \\ -K\rho z e^{-T_i/T} \end{pmatrix} \tag{1.1}$$

describing the motion of a fluid in the x-y plane in which a one step irreversible chemical reaction is taking place. Initial data is given at $t = 0$. The dependent variables $\rho(x,y,t), m(x,y,t), n(x,y,t), e(x,y,t)$ $z(x,y,t)$ are the density, x- and y-momentum, energy and the fraction of unreacted fluid respectively. The pressure is given by

$$p = (\gamma - 1)(e - \frac{1}{2}(m^2 + n^2)/\rho - q_0 \rho z)$$

and the temperature is defined as $T = p/\rho$. We will use $u = m/\rho$ to denote the velocity.

We will sometimes use (1.1) with only one space dimension present. We have neglected heat transfer and viscos effects. We will focus on the discontinuous solutions of detonation waves. For these waves the viscosity is not as important as for the slower deflagration wave solutions.

The parameters q_0, T_i, γ, K correspond to chemical heat release, ignition temperature, c_p to c_v ratio, and an equilibrium constant respectively. The equations have

[1] Department of Mathematics, UCLA, Los Angeles, CA 90024.
Research supported by ONR grant N00014-86-K-0691, NSF grant DMS 88-11863, NASA grant NCC 2-374.

[2] Department of Scientific Computing, Uppsala University, S-75223 Uppsala, Sweden.
Research supported by ONR grant N00014-86-K-0691.

been non dimensionalized, leaving the choice of these four parameters to completely determine the problem.

We refer to (1.1) as the reactive Euler equations with Arrhenius kinetics. We will also consider (1.1) with

$$-K\rho z e^{T_i/T} \tag{1.2}$$

replaced by

$$-K\rho z H(T_i - T), \tag{1.3}$$

where $H(x) = 1$ for $x > 0$ and $H(x) = 0$ for $x < 0$. We will refer to this variant of (1.1) as the reactive Euler equations with Heaviside kinetics.

In some applications it is appropriate to use the source term

$$-K\rho z T^{\alpha} e^{-T_i/T} \tag{1.4}$$

with $\alpha \neq 0$, instead of the one in (1.1). The shape of the traveling wave is affected by the choice of source term. See examples in section 4.

Our objective in this paper is to study numerical methods for these equations. We shall present two algorithmic innovations. A new class of higher order approximations and a technique for robust treatment of stiffness problems at detonation fronts.

One difficulty in the approximation is the rapid dynamical behavior and the steep gradients of the detonation front. In section 2 we shall introduce a class of efficient shock capturing methods for the 1-dimensional version of (1.1). We investigate the properties of the methods for different order of approximations and different choices of flux limiters. Details for the implementation of the algorithms in both 1 and 2 space dimensions are given in the appendix.

Another difficulty is that a shock wave and a thin combustion layer are located close to each other in the solution. Modern shock capturing methods can be made to deal with the shock wave and stiff ODE solvers can handle the source term when K is large. There are, however, remaining stiffness problems, due to the interaction between these two parts of the solution algorithm. It is well known [2,5,10] that for certain parameter values, non physical waves will occur. This spurious numerical wave is initiated by the numerical shock profile. Even a modern shock capturing method will have a few grid points in the shock profile and the corresponding temperature values may trigger a too early chemical reaction [5].

In section 3 we shall present a robust technique which guarantees that no strong chemical reaction starts before the shock wave has passed. The technique is based on extrapolation of the source term and we indicated this idea in [13] for a model problem. Most of [13] deals with a projection technique which is another method for avoiding the same numerical problem. The projection technique is, however, not easy to extend to systems.

Numerical results for the new methods are presented in sections 4 and 5 for the one and two dimensional problems respectively.

A theoretical study of the numerical properties of the extrapolation technique when applied to simple model problems is given in [6].

2. Shock capturing methods. We shall describe the one dimensional setting for the method. Two space dimensions is implemented analogously (see also appendix A). We introduce the grid points $x_j, j = \ldots, -1, 0, 1, \ldots$, with equal mesh spacing $\Delta x = x_{j+1} - x_j$. The time levels $t_0, t_1, \ldots$ are also uniformly spaced with space step $\Delta t = t_{n+1} - t_n$. We use u_j^n either to denote the approximate solution in the point (x_j, t_n), or sometimes to denote the approximate cell average of u in the cell $[x_{j-1/2}, x_{j+1/2}]$ at time t_n. The difference between cell averages and point values is significant only for order of accuracy three and higher.

The convective flux derivative

$$\begin{pmatrix} m \\ \rho u^2 + p \\ m(e+p)/\rho \\ mz \end{pmatrix}_x$$

is discretized in space, using an upwind method. Godunov's and Roe's [8] methods are implemented. In the computations almost no difference in the results obtained with the two methods were observed. The numerical results presented in the following sections, was computed using Roe's method, because it is easier to vectorize and thus gave lower execution time on the Alliant FX computer. On a scalar computer there is no significant difference in execution time between Godunov's and Roe's method.

The convective part of the equations deviates very little from the non reactive Euler equations, since the extra equation appears as an additional linear field in the characteristic variables. A detailed description of the formulas used to implement Roe's method is given in appendix A.

Higher order accuracy was obtained using piecewise polynomial interpolation of ENO type, [8]. Piecewise linear and piecewise parabolic reconstruction were implemented. In the problems solved here, it turned out that the interpolation in the physical variables, instead of using characteristic variables, was sufficient to produce a good solution. A TVD limiter function was used to the limit the slopes in the piecewise linear reconstruction.

In summary, the problem after flux discretization is on the form

$$\frac{du_j(t)}{dt} + \frac{h_{j+1/2} - h_{j-1/2}}{\Delta x} = g(u_j(t))$$

where

$$h_{j+1/2} = h(u_{j+1}^-(t), u_j^+(t))$$

with $h(u, v)$ the first order numerical flux function, and u_j^+, u_j^- are the values of u at the left and right ends of cell j obtained from the piecewise polynomial interpolation.

For the time discretization, a Runge-Kutta method is used. It is well known [12], that the second order method

$$\begin{aligned} u^{(1)} &= u^n - \lambda \Delta_+ h_{j-1/2}^n \\ u^{(2)} &= u^{(1)} - \lambda \Delta_+ h_{j-1/2}^{(1)} \\ u^{n+1} &= (u^n + u^{(2)})/2 \end{aligned}$$

for the convective terms gives a good performance with respect to shocks. Here $h_{j-1/2}$ is the numerical flux function described above, and we use $\lambda = \Delta t/\Delta x$. The source term is added such that it does not impose any additional stability restrictions and such that the accuracy is the same as for the convective method (two). We therefore consider the following method

$$\begin{aligned} u^{(1)} &= u^n - \lambda\Delta_+ h^n_{j-1/2} + a\Delta t g(u^n) + b\Delta t g(u^{(1)}) \\ u^{(2)} &= u^{(1)} - \lambda\Delta_+ h^{(1)}_{j-1/2} + c\Delta t g(u^{(1)}) + d\Delta t g(u^{(2)}) \\ u^{n+1} &= (u^n + u^{(2)})/2 \end{aligned}$$

where $g(u)$ is the source term. It is easy to derive the following one parameter family of second order accurate methods,

$$a = 1 - b, \quad c = 1 + b, \quad d = -b.$$

For example the explicit method $a = 1, b = 0, c = 1, d = 0$ is included in this family. By performing standard ODE stability analysis on the problem with $h_{j-1/2} = 0, g(u) = \lambda u$, it turns out that the only choice which contains the entire left hand plane in the stability region (A stability) is

$$a = 1/2, \quad b = 1/2, \quad c = 3/2, \quad d = -1/2.$$

(With no convection, this method yields third order accuracy for the source term.) This is the method used for implicit treatment of the source term.

For the third order ENO discretization of the convective fluxes, we used a third order Runge-Kutta method for time discretization. This is another of the so called TVB-Runge-Kutta methods derived in [12]. Similar to the second order case we add the source term to this method to obtain

$$\begin{aligned} u^{(1)} &= u^n - \lambda\Delta_+ h^n_{j-1/2} + a\Delta t g(u^n) + b\Delta t g(u^{(1)}) \\ u^{(2)} &= \frac{3}{4}u^n + \frac{1}{4}(u^{(1)} - \lambda\Delta_+ h^{(1)}_{j-1/2}) + c\Delta t g(u^{(1)}) + d\Delta t g(u^{(2)}) \\ u^{n+1} &= \frac{1}{3}u^n + \frac{2}{3}(u^{(2)} - \lambda\Delta_+ h^{(2)}_{j-1/2}) + e\Delta t g(u^{(2)}) + f\Delta t g(u^{n+1}) \end{aligned}$$

A straightforward but lengthy analysis reveal that the following values

$$a = 1, \quad b = 0, \quad c = -3/4, \quad d = 1, \quad e = 0, \quad f = 2/3$$

give overall third order accuracy, and A-stability for the method with convective terms equal to zero. A further analysis yields that the method is $A(\alpha)$ stable for the source term, when the convective term satisfies a CFL condition. We will not present the analysis of these Runge-Kutta splitting methods here, instead they will be treated in full length in a forthcoming paper.

The piecewise polynomial reconstruction method used is based on cell averages, and since

$$g(\frac{1}{\Delta x}\int_{x_{j-1/2}}^{x_{j+1/2}} u\,dx) = \frac{1}{\Delta x}\int_{x_{j-1/2}}^{x_{j+1/2}} g(u)\,dx + O(\Delta x^2)$$

it is necessary to change the right hand side treatment for accuracy greater than two.

We have used Simpson's rule to get the approximation

$$(g(v^n_{j+1/2}) + 4g(v^n_j) + g(v^n_{j-1/2}))/6$$

for the right hand side on the explicit time level. Here $v^n_{j+1/2}, v^n_j, v^n_{j-1/2}$ are point values, obtained from the piecewise parabolic ENO reconstruction from the cell averages u^n_j. The implicit part of the right hand side was implemented only to second order accuracy. It is necessary to treat the source term implicitly for problems with very stiff chemistry. It is an easy calculation to show that the nonzero eigenvalue of the linearized right hand side is

$$\lambda_s = Ke^{-T_i/T}((\gamma - 1)q_0 z\frac{T_i}{T^2} - 1)$$

if Arrhenius kinetics is used. The convective part of the equations has the maximum eigenvalue

$$\lambda_c = u + c$$

Thus if

$$\Delta t\lambda_c/\Delta x < \Delta t\lambda_s \tag{2.1}$$

the source term will impose an additional restriction on the time step, unless approximated implicitly (assuming for simplicity a CFL stability limit of one). Note that a large K will lead to a small Δt, but when $K\Delta t \to 0$, and $\Delta t/\Delta x =$ constant, the CFL restriction from the convective part will dominate. Condition (2.1) will have to be checked for each particular problem, some applications will require an implicit method and some will not.

It is possible to prove, by elementary calculus, that the ratio λ_s/λ_c is bounded from above, with a bound depending on the parameters K, T_i, γ, q_0.

An implicit method for the source term means that a non linear equation has to be solved in each grid point. The equation is (with X as unknown)

$$X = (\rho z)^n_j - \lambda\Delta_+ h^n_{j-1/2} - K\Delta t X e^{-T_i/T^{n+1}_j} \tag{2.2}$$

where

$$T^{n+1}_j = (\gamma - 1)(e^{n+1}_j/\rho^{n+1}_j - \frac{1}{2}(u^{n+1}_j)^2 - q_0 X/\rho^{n+1}_j).$$

The functions e, ρ, u are already know at t_{n+1} from the three equations without source terms. By elementary calculus it is possible to show that there is always one root $X \in [0, \rho^{n+1}_j]$ if the convective step guarantees that $(\rho z)^n_j - \lambda\Delta_+ h^n_{j-1/2} \in [0, \rho^n_j]$. We solve (2.2) using Newton's method.

It is possible to avoid solving (2.2) numerically, if we neglect the dependence of the temperature on X. We can then solve (2.2) analytically. The numerical experiments showed this approximation to lead to stiffness problems and is thus *not* recommended.

In the case of Heaviside kinetics, (2.2) takes the simpler form

$$X = (\rho z)^n_j - \lambda\Delta_+ h^n_{j-1/2}, \quad T^{n+1}_j < T_i$$
$$X = (\rho z)^n_j - \lambda\Delta_+ h^n_{j-1/2} - K\Delta t X, \quad T^{n+1}_j > T_i$$

We solve this analytically to get

$$
\begin{aligned}
&X = (\rho z)_j^n - \lambda \Delta_+ h_{j-1/2}^n, \quad T^{n+1} < T_i \\
&X = ((\rho z)_j^n - \lambda \Delta_+ h_{j-1/2}^n)/(1 + K\Delta t), \quad T^{n+1} > T_i
\end{aligned}
\tag{2.3}
$$

Since X decreases when T becomes larger than T_i, we will get the same result if the test $T^{n+1} > T_i$ is replaced by $T^n > T_i$, thereby making it unnecessary to solve any non linear equation.

3. The extrapolation method. Numerical results for the problem with Heaviside kinetics is well known to be sensitive to the size of $K\Delta t$ [2,5,13].

In figures 3.1 and 3.2 we show the density and mass fraction unreacted fluid, computed with Heaviside kinetics using $K = 10000$ and $K = 100$ respectively. The other parameter values were $T_i = 3, q_0 = 50, \gamma = 1.2$. We started with $p = 1, u = 0, \rho = 1$ to the right and obtained the initial profile by integration of an ODE as described in section 4. Chapman- Joguet conditions were used to determine the wave speed. The larger K value causes an unphysical wave, which moves with wrong speed. For the smaller K value, the solution profile is well resolved and a correct solution is obtained. See [2,5] for similar results.

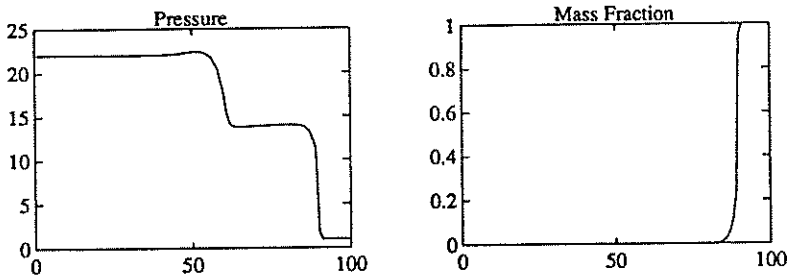

figure 3.1, K=10000

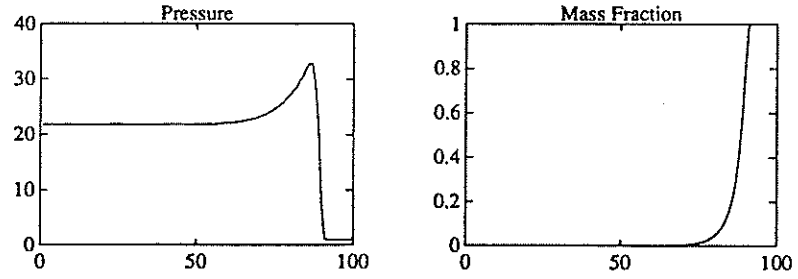

figure 3.2, K=100

This effect stems from the computation of the source term. It can be seen from (2.4) that if $K\Delta t$ is large, then ρz will drop to zero immediately as T increases above T_i. All shock capturing methods will give a few grid points in the shock. This results in a local error of order 1 in the temperature. The error may trigger the chemistry at a wrong location. If, e.g. the difference method places one new point in the shock at each time step, the chemical reaction will propagate with one grid point per time step. Note that the method for the source term is backward Euler, an unconditionally stable method for the ODE.

We shall now show how to avoid this stiffness problem. A detonation wave consists of a non reacting shock wave which first increases the temperature of the fuel mixture, so that ignition occurs behind the shock wave. No chemical reactions start before the shock wave has passed through. We shall emulate this behavior in the numerical method. Numerically, there are always a few grid points in the shock. We want to make sure that none of the points inside the numerical shock triggers the chemistry. One simple way of ensuring this is to evaluate the right hand side a few grid points ahead of the shock. i.e. instead of solving (2.2) we solve

$$X = (\rho z)_j^n - \lambda \Delta_+ h_{j-1/2}^n - K \Delta t X e^{-T_i/T_{j+d}^{n+1}} \tag{3.1}$$

where now

$$T_{j+d}^{n+1} = (\gamma - 1)(e_{j+d}^{n+1}/\rho_{j+d}^{n+1} - \frac{1}{2}(u_{j+d}^{n+1})^2 - q_0 X/\rho_j^{n+1}) \tag{3.2}$$

and d is the number of points in the shock, usually one or two. The accuracy will drop to first order, but higher order accuracy can be recovered by an extrapolation in the temperature, i.e. by using

$$2T_{j+1}^{n+1} - T_{j+2}^{n+1}$$

in place of T_{j+d}^{n+1} inside the exponentiation in (3.1). Here T_{j+1}^{n+1} and T_{j+2}^{n+1} depend on X through (3.2).

During the computations, we sometimes found that (3.1) had no solution, in such a case the following approximation was used,

$$X = (\rho z)_j^n - \lambda \Delta_+ h_{j-1/2}^n \tag{3.3}.$$

We tried other choices of X in case of such a failure, but no visible difference from using (3.3) were seen.

In the formulas above, we have assumed that the detonation travels from the left to the right, so that the solution at $j+1$ have lower temperature than the solution at j. In a more general situation and in more than one space dimension, the direction of extrapolation is determined as the direction of decreasing temperature.

The extrapolations of values in the source terms are similar to the extrapolations in the subcell resolution method by Harten [7]. In [7] all variables are extrapolated into the computational cell. This approach works very well in one dimension but has so far been difficult to extend to multidimensional problems.

It would have been possible to use a more complicated algorithm. We could e.g. have used a sensor to indicate if a certain point is inside the shock layer, and modify the chemistry only at those points. The method described above is however simpler and works well, so we found no need to develop a more complicated method.

4. Numerical results in one space dimension. The test problems solved in this and next section have been chosen as suitable for comparing numerical methods, and not for solving a particular applied problem in combustion. They do however, capture features present in more realistic problems.

Below we show some traveling wave solutions to the one dimensional problem corresponding to (1.1) with different kind of chemical terms, where the data are chosen to

yield a single Chapman-Joguet detonation wave. In general, to find a traveling wave solution to

$$u_t + f(u)_x = g(u) \tag{4.1}$$

we insert the ansatz $u = u(x - st)$, into (4.1). The result is the ODE

$$(s - f'(u))u' = g(u)$$

which we solve using a numerical ODE solver. s is given initially by the jump conditions.

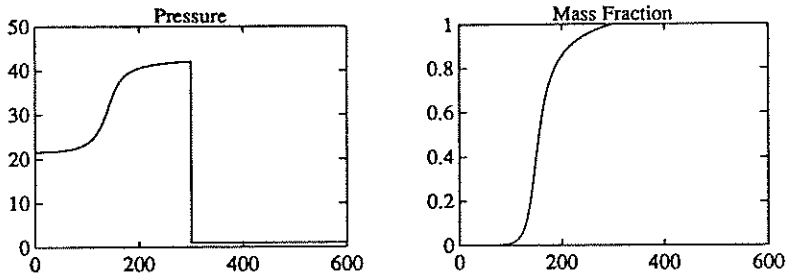

figure 4.1, Arrhenius kinetics (1.2)

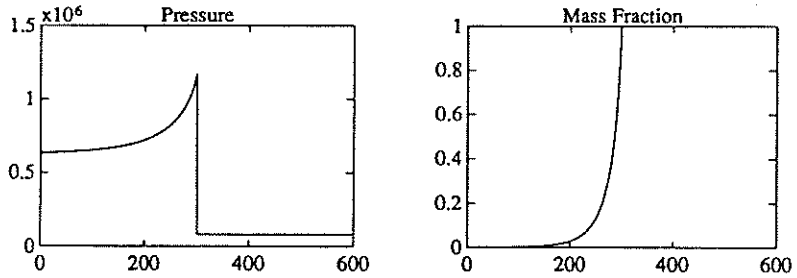

figure 4.2, Heaviside kinetics (1.3)

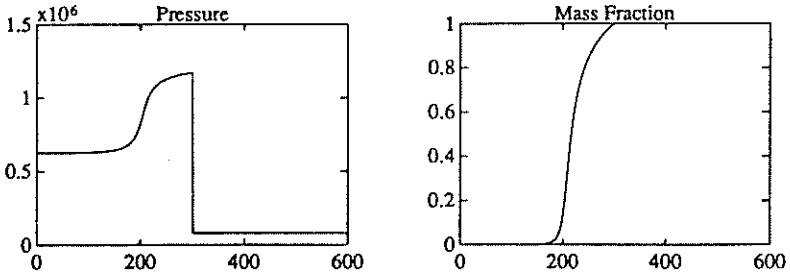

figure 4.3, Arrhenius with $\alpha = 2.5$ kinetics (1.4)

Note that the Heaviside kinetics gives a qualitatively different wave profile without inflection point. The Arrhenius kinetics have a flat part behind the shock wave, the induction zone. The chemical reaction occurs on the negative flank after induction zone, while in the Heaviside kinetics, the reaction starts immediately at the shock front. This explains why the stiffness problem encountered in numerical methods (see section 3) tends to be worse for the Heaviside kinetics. We also conclude that the shape of the solution is not influenced by the factor $T^{2.5}$.

Below we have made the same computation with Heaviside kinetics as in figures 3.1 and 3.2, but now with the source term extrapolated from two grid point out ($d = 2$ in (3.1)).

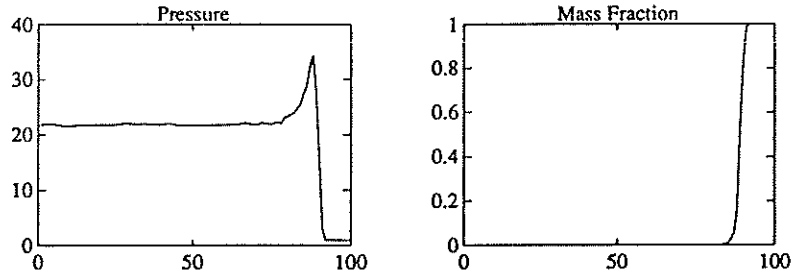

figure 4.4, K=10000

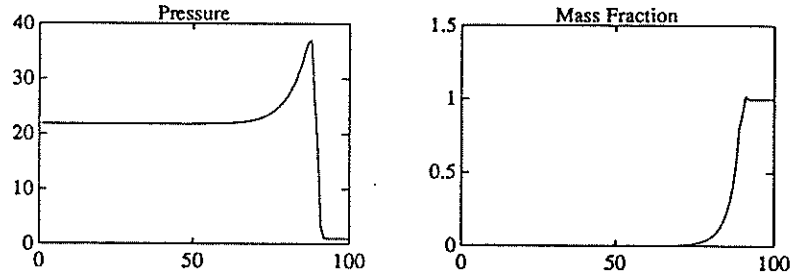

figure 4.5, K=100

The unphysical waves for $K = 10000$ (fig. 3.1) has disappeared and the solution for $K = 100$ is not seriously affected by the small error deriving from the extrapolation of the source term.

Next we shall investigate how well we can capture the behavior of the peak pressure at the ZND spike. It is possible to increase the pressure in the left hand state, and thereby give the detonation wave a so called overdrive. For a detonation moving with speed s, the overdrive, f, is defined as $f = (s/s_{CJ})^2$ where s_{CJ} is the speed of a Chapman-Joguet detonation. Thus we always have $f \geq 1$, since weak detonations are not physically admissible. For certain values of f the pressure peak is oscillating in a periodic way, for other values it is stable, and for some values it is oscillating in a chaotic way. For an analysis of these phenomena, see [1,3].

To capture this oscillatory behavior a large number of grid points is usually required. We next investigate how the resolution required is affected by the accuracy of the method used.

We here use the parameter values $T_i = 50, q_0 = 50, \gamma = 1.2, K = 10000$ and Arrhenius kinetics. The values are taken from [1] and [3] (except for K). An overdrive, $f = 1.6$, was given, a value corresponding to a case where the pressure peak oscillates periodically [1,3]. We compute on a domain of length 1, which is moved along with the wave. Initially the exact ZND profile is given by solving the traveling wave problem using a fourth order Runge-Kutta method. The boundary values are given as $p = 1, \rho = 1, u = 0$ to the right and extrapolated ($w_0 = w_1$) to the left, the wave travels to the right. All computations were run to time = 1.

Below we compare a few different numerical methods, one first order and two second order TVD schemes with different flux limiters and one third order ENO scheme. We did

not use extrapolation of the source term in these computations. We used explicit time discretization of the source term, since condition (2.1) showed that the CFL condition for the convective part of the equations was sufficient to ensure stability for the overall method. For the second order scheme, we compare results from using the minmod flux limiter and van Leer's flux limiter [14].

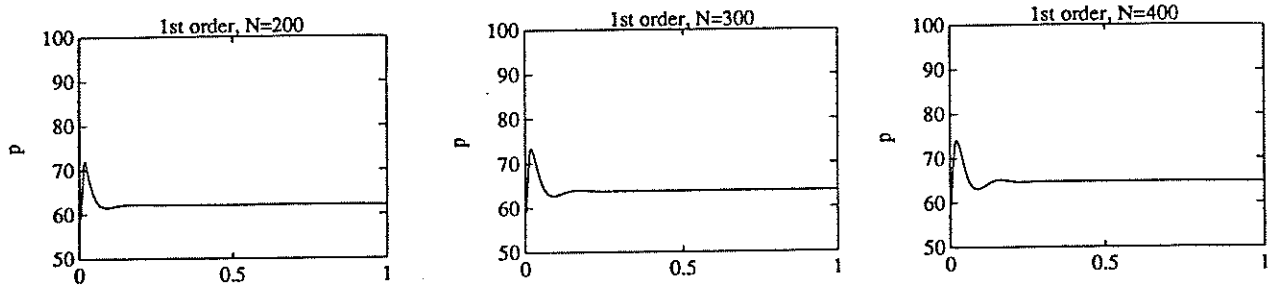

f=1.6, 200 points f=1.6, 300 points f=1.6, 400 points

figure 4.6 First order TVD method

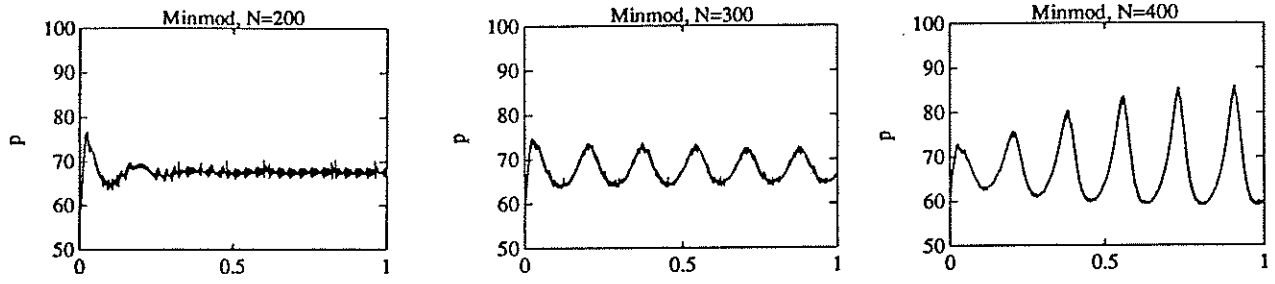

f=1.6, 200 points f=1.6, 300 points f=1.6, 400 points

figure 4.7 Second order TVD, minmod limiter

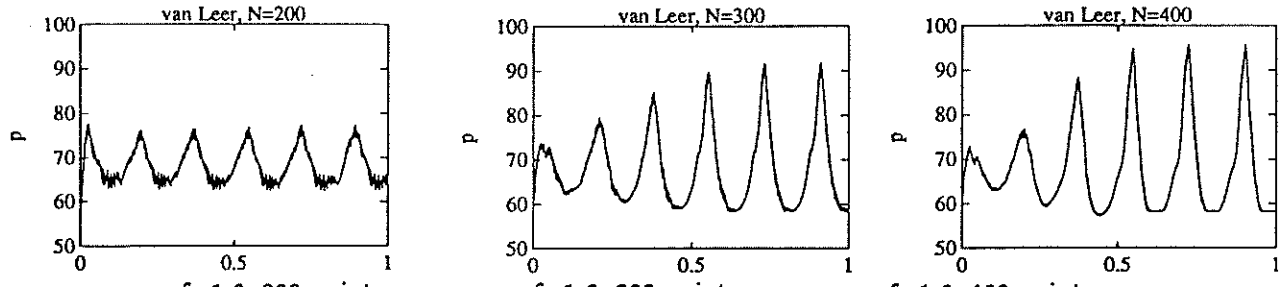

f=1.6, 200 points f=1.6, 300 points f=1.6, 400 points

figure 4.8 Second order TVD, van Leer's limiter

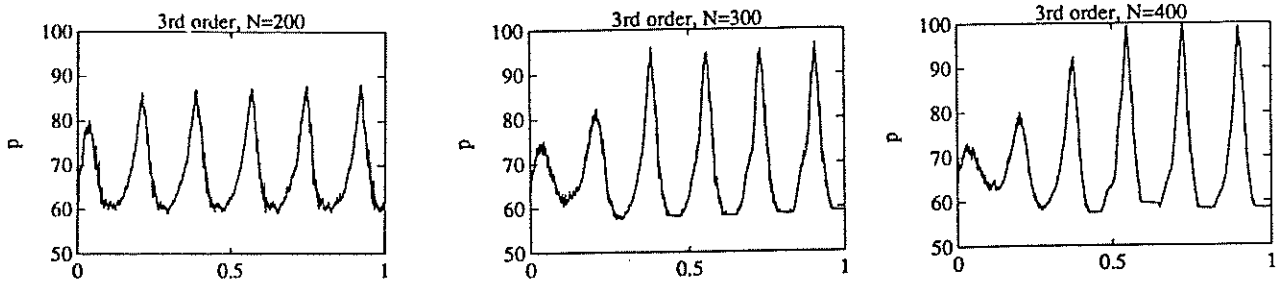

f=1.6, 200 points f=1.6, 300 points f=1.6, 400 points

figure 4.9 Third order ENO

The first order scheme can not capture the correct behavior, not even on the finest grid. This is hardly surprising, first order schemes are too dissipative. It is more interesting to note the difference deriving from different flux limiters in the second order methods. With van Leer's limiter, we can capture the right frequency, (but not amplitude) with as few as 200 grid points, while the minmod limiter requires at least 300 grid points for a similar resolution. The third order scheme performs best, we get a solution with both frequency and amplitude reasonably well represented using 200 grid points.

We did not use the half reaction time as time unit. Nevertheless, by numerical integration of the steady solution profile, we found that $t_{1/2} = 0.0212$ and the corresponding half reaction length $\Delta_{1/2} = 0.0193$. This means that 200 grid points corresponds to roughly 4 points per half reaction length, this seems to be the fewest possible number of points required to capture the oscillations using the best (3rd order) method. The period of the oscillations is 8 half reaction times, in accordance with previous results [1,3].

In order to capture the dynamics correctly the time step had to be chosen so small that no instability of the type in figure 3.1 occurred. The extrapolation technique was thus not needed. Low order extrapolation introduces local truncation errors which may interfere with the dynamics.

5. Numerical results in two space dimensions. Computations of a two dimensional traveling detonation wave are presented. We used a second order TVD method in all computations in this section.

Consider a two dimensional channel of width 1/2, the upper and lower boundaries are solid walls. We start a with a ZND profile in the x direction, but given a slightly curved shape through a sinusodial perturbation,

$$u_0(x,y) = w(x + \Delta x \sin 2\pi(y + \frac{1}{4}))$$

where $w(x)$ is the one dimensional detonation wave. See figure 5.1 for the initial data.

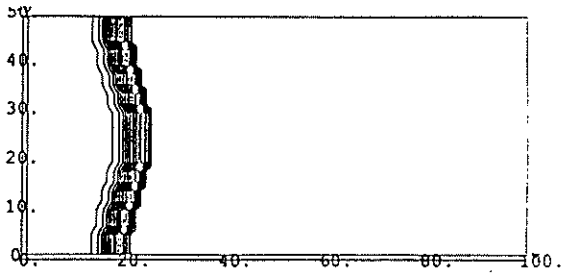

figure 5.1 density contours

The solution was computed on grid of 100×50 points which was moved along with the detonation wave. We solved equations (1.1) with Arrhenius kinetics, and parameter values $T_i = 50, q_0 = 50, \gamma = 1.2, K = 10000$. To the right, we give the freestream values $p = 3, \rho = 1, u = 0$ and the ZND profile $w(x)$ is obtained by numerical integration as in the one dimensional computations.

The figure below (5.2) shows density contours at six different times.

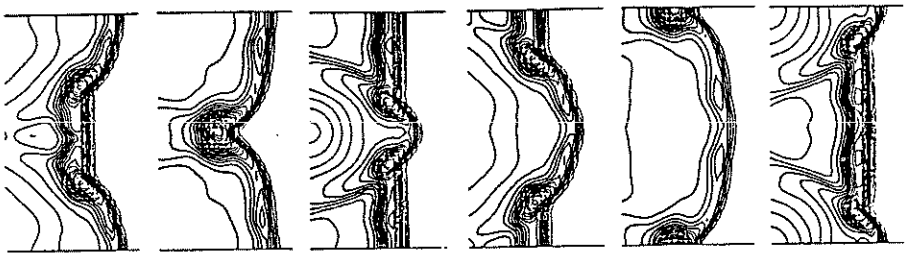

figure 5.2 density contours

One important feature of this solution is the triple points, which travel in the transverse direction and bounces back and forth against the upper and lower walls.

An discussion of the mechanisms driving this solution is given in [9]. The trace of the triple points can be seen in experiments with smoked screens as a cellular pattern [4]. By plotting contour lines in the y-t plane we can obtain a similar pattern for our numerical solution. The figure below shows 7 detonation cells.

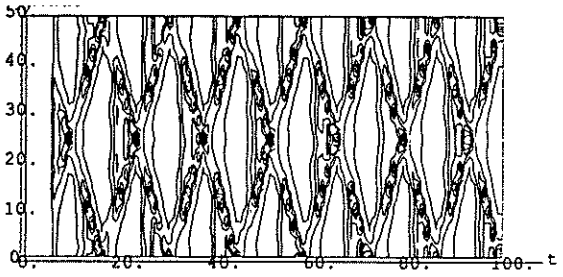

figure 5.3 density contours in the y-t plane

The CFL number in this computation was 0.4. We next increase the time step by taking a CFL number of 0.85. The solution at six different times are showed in figure 5.4

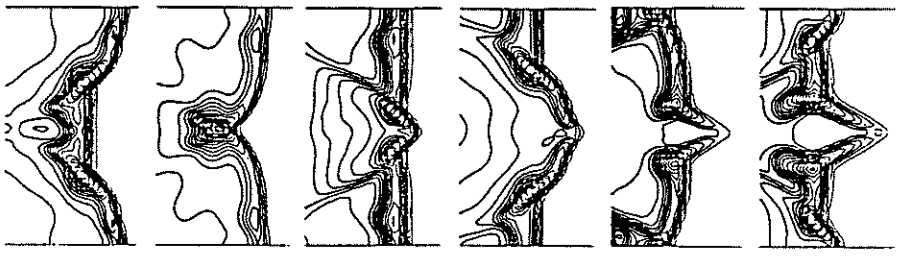

figure 5.4 density contours

After some time the triple points cease to move, and a triangular shape extends from the detonation front. In the y-t plane in figure 5.5 it is clearly seen that the triple point dynamics ceases.

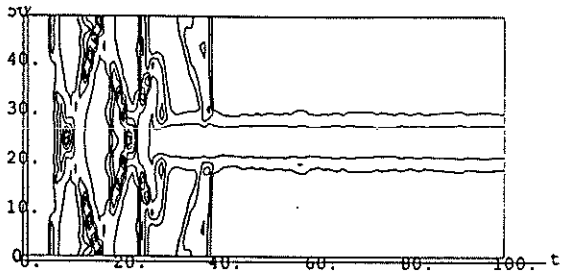

figure 5.5 density contours in the y-t plane

The solution is completely wrong, due to stiffness problems. The modified method will help to overcome this difficulty, as we show next. In figure 5.6 we display the same computation as in 5.4, but with the source term extrapolated, using $d = 1$. The direction of extrapolation is taken from the lowest temperature direction as described in section 3. There is no artificial numerical detonation spike.

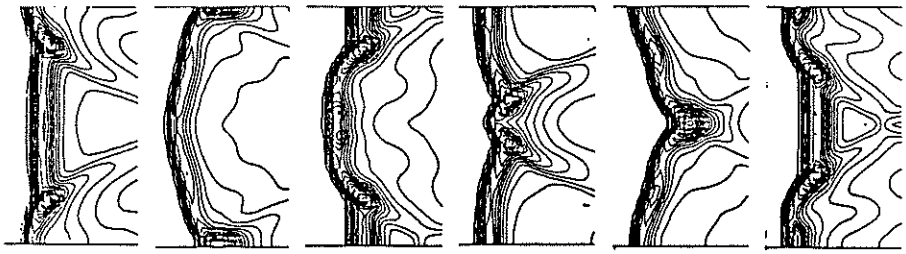

figure 5.6 density contours

The dynamics is recovered and the solution have the same structure as the one computed with smaller time step (figure 5.2). From the y-t plane plot, we conclude that the detonation cell sizes deviate very little from the solution in figure 5.3.

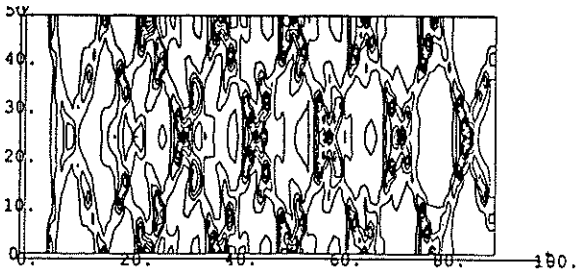

figure 5.7 density contours in the y-t plane

References

[1] G.E.Abouseif and T.Y.Toong "Theory of Unstable One-Dimensional Detonations" Combust. Flame **45**, (1982), pp.67–94.

[2] M.Ben-Artzi, "The Generalized Riemann Problem for Reactive Flows", J. Comp. Phys., **81**, (1989), pp.70–101.

[3] A.Bourlioux, A.Majda, and V.Roytburd "Theoretical and Numerical Structure for Unstable One-Dimensional Detonations", SIAM, J. Appl. Math, to appear.

[4] D.C.Bull, J.E.Elsworth, P.J.Shuff, and E.Metcalfe "Detonation Cell Structures in Fuel/Air Mixtures", Combust. Flame **45**, (1982), pp.7–22.

[5] P.Colella, A.Majda, and V.Roytburd "Theoretical and Numerical Structures for Reacting Shock Waves", SIAM J.Sci.Stat.Comput. **7**, (1986), pp.1059–1080

[6] B. Engquist and B. Sjögreen, "Difference Methods for Nonlinear Conservation Laws with Stiff Terms", to appear.

[7] A. Harten, "ENO Schemes with Subcell Resolution", J. Comput. Phys., **83** (1989), pp. 148-184.

[8] A. Harten, S. Osher, B.Engquist, and S.Chakravarthy "Some Results on Uniformly High-Order Accurate Essentially Nonoscillatory Schemes", Applied Numerical Mathematics **2** (1986), pp.347–377

[9] K.Kailasanath, E.S.Oran, J.P.Boris, and T.R.Young "Determination of Detonation Cell Size and the Role of Transverse Waves in Two-Dimensional Detonations", Combust. Flame **61**, (1985), pp.199–209.

[10] R.J. LeVeque and H.C. Yee, "A Study of Numerical Methods for Hyperbolic Conservation Laws with Stiff Source Terms", J. Comput. Phys., **86** (1990), pp. 187-210.

[11] P. L. Roe, "Approximate Riemann solvers, parameter vectors, and difference schemes", J. Comput. Phys., **43** (1981), pp. 357–372.

[12] C-W Shu and S.Osher, "Efficient Implementation of Essentially Non-oscillatory Shock-Capturing Schemes", J. Comput. Phys. **77** (1988), pp.439–471.

[13] B. Sjögreen and B. Engquist, "Numerical Approximation of Hyperbolic Conservation Laws with Stiff Terms", Proc. Third International Conf. on Hyperbolic Problems, to appear.

[14] P.Sweby, "High Resolution Schemes Using Flux Limiters for Hyperbolic Conservation Laws", SIAM, J. Numer. Anal. **21** (1984), pp.995–1010.

Appendix A.

We shall give the eigendecomposition necessary for Roe's approximate Riemann solver. We assume that γ is constant. Consider the system without source term

$$\begin{pmatrix} \rho \\ m \\ e \\ \rho z \end{pmatrix}_t + \begin{pmatrix} m \\ \rho u^2 + p \\ m(e+p)/\rho \\ mz \end{pmatrix}_x = \begin{pmatrix} 0 \\ 0 \\ 0 \\ 0 \end{pmatrix}.$$

The Jacobian of the flux function has the eigenvalues

$$\lambda_1 = u - c, \quad \lambda_2 = u, \quad \lambda_3 = u, \quad \lambda_4 = u + c$$

where $u = m/\rho$ and $c^2 = \gamma p/\rho$. The corresponding right eigenvectors are

$$\mathbf{r}_1 = \begin{pmatrix} 1 \\ u-c \\ h-uc \\ z \end{pmatrix} \quad \mathbf{r}_2 = \begin{pmatrix} 1 \\ u \\ u^2/2 \\ 0 \end{pmatrix} \quad \mathbf{r}_3 = \begin{pmatrix} 1 \\ u \\ u^2/2 + q_0 \\ 1 \end{pmatrix} \quad \mathbf{r}_4 = \begin{pmatrix} 1 \\ u+c \\ h+uc \\ z \end{pmatrix}$$

where $h = (e+p)/\rho$. There is a one parametric freedom in the choice of $\mathbf{r}_2$ and $\mathbf{r}_3$. It is also necessary to solve the linear system of equations

$$(r_1 r_2 r_3 r_4)\alpha = \Delta \mathbf{u}.$$

The formulas to do this are

$$\begin{aligned}
\alpha_1 &= (\gamma-1)/(2c^2)(\Delta e + 1/2u^2\Delta\rho - u\Delta m - q_0\Delta(\rho z)) - (1/(2c)(\Delta m - u\Delta\rho) \\
\alpha_4 &= (\Delta m - u\Delta\rho)/c + \alpha_1 \\
\alpha_3 &= \Delta(\rho z) - z\alpha_4 - z\alpha_1 \\
\alpha_2 &= \Delta\rho - \alpha_1 - \alpha_3 - \alpha_4
\end{aligned}$$

In Roe's Riemann solver, the eigendecomposition is evaluated at a weighted average in the same way as for the Euler equations, i.e.

$$\begin{aligned}
u &= wu_j + (1-w)u_{j+1} \\
h &= wh_j + (1-w)h_{j+1} \\
z &= wz_j + (1-w)z_{j+1}
\end{aligned}$$

where $w = \sqrt{\rho_j}/(\sqrt{\rho_{j+1}} + \sqrt{\rho_j})$. This gives the desired property

$$\mathbf{f}_{j+1} - \mathbf{f}_j = A_{j+1/2}(\mathbf{u}_{j+1} - \mathbf{u}_j)$$

for the eigendecomposed matrix $A_{j+1/2}$.

We next list the eigenvectors and eigenvalues for the two dimensional problem (1.1). On a variable grid, metric coefficients enter into the equations and we are led to consider

the flux function

$$\alpha\mathbf{F}+\beta\mathbf{G}=\alpha\begin{pmatrix} m \\ m^2/\rho+p \\ mn/\rho \\ m(e+p)/\rho \\ mz \end{pmatrix}+\beta\begin{pmatrix} n \\ mn/\rho \\ n^2/\rho+p \\ n(e+p)/\rho \\ nz \end{pmatrix}$$

with $\mathbf{F}$ and $\mathbf{G}$ the x and y direction fluxes in (1.1) respectively and α,β represents the metric. We define

$$u=m/\rho,\quad v=n/\rho,\quad p=(\gamma-1)(e-\frac{1}{2}\rho(u^2+v^2)-q_0\rho z)$$

The eigenvalues of the jacobian of $\alpha\mathbf{F}+\beta\mathbf{G}$ are

$$\lambda_1=\bar{u}-sc,\quad \lambda_2=\lambda_3=\lambda_4=\bar{u},\quad \lambda_5=\bar{u}+sc$$

with $\bar{u}=\alpha u+\beta v$ and $s=\sqrt{\alpha^2+\beta^2}$. The eigenvectors are

$$\mathbf{r}_1=\begin{pmatrix} 1 \\ u-k_1c \\ v-k_2c \\ h-\hat{u}c \\ z \end{pmatrix}\quad \mathbf{r}_2=\begin{pmatrix} 1 \\ u-k_2c \\ v+k_1c \\ q^2/2-k_2uc+k_1vc+q_0 \\ 1 \end{pmatrix}\quad \mathbf{r}_3=\begin{pmatrix} 1 \\ u \\ v \\ q^2/2 \\ 0 \end{pmatrix}$$

$$\mathbf{r}_4=\begin{pmatrix} 1 \\ u+k_2c \\ v-k_1c \\ q^2/2+k_2uc-k_1vc+q_0 \\ 1 \end{pmatrix}\quad \mathbf{r}_5=\begin{pmatrix} 1 \\ u+k_1c \\ v+k_2c \\ h+\hat{u}c \\ z \end{pmatrix}$$

with the definitions

$$k_1=\alpha/\sqrt{\alpha^2+\beta^2},\quad k_2=\beta/\sqrt{\alpha^2+\beta^2},$$
$$\hat{u}=k_1u+k_2v,\quad q^2=u^2+v^2,\quad c^2=\gamma p/\rho$$

The eigenvectors are independent, since

$$Det(\mathbf{r}_1\ \mathbf{r}_2\ \mathbf{r}_3\ \mathbf{r}_4\ \mathbf{r}_5)=4c^4/(\gamma-1)$$

To solve the system of equations

$$(\mathbf{r}_1\ \mathbf{r}_2\ \mathbf{r}_3\ \mathbf{r}_4\ \mathbf{r}_5)\begin{pmatrix} x_1 \\ \dots \\ x_5 \end{pmatrix}=\begin{pmatrix} d\rho \\ dm \\ dn \\ de \\ dy \end{pmatrix}$$

define

$$a_1 = \frac{\gamma-1}{c^2}(de + \frac{q^2}{2}d\rho - udm - vdn - q_0 dy)$$
$$a_2 = k_1\frac{dm - ud\rho}{c} + k_2\frac{dn - vd\rho}{c}$$
$$a_3 = k_2\frac{dm - ud\rho}{c} - k_1\frac{dn - vd\rho}{c}$$

then the solution is

$$x_1 = \frac{a_1 - a_2}{2}$$
$$x_2 = \frac{dy - za_1 - a_3}{2}$$
$$x_4 = x_2 + a_3$$
$$x_5 = \frac{a_1 + a_2}{2}$$
$$x_3 = d\rho - (x_1 + x_2 + x_4 + x_5)$$

To do ENO reconstruction in the characteristic variables and to implement far field boundary conditions, the left eigenvectors are required. They are

$$\mathbf{l}_1^T = \frac{1}{2c^2}\begin{pmatrix} \hat{u}c + (\gamma-1)\frac{q^2}{2} \\ -k_1 c - (\gamma-1)u \\ -k_2 c - (\gamma-1)v \\ \gamma - 1 \\ -(\gamma-1)q_0 \end{pmatrix}, \quad \mathbf{l}_2^T = \frac{1}{2c^2}\begin{pmatrix} \hat{v}c - (\gamma-1)z\frac{q^2}{2} \\ -k_2 c + (\gamma-1)uz \\ k_1 c + (\gamma-1)vz \\ -(\gamma-1)z \\ c^2 + (\gamma-1)q_0 z \end{pmatrix}$$

$$\mathbf{l}_3^T = \frac{1}{2c^2}\begin{pmatrix} 2c^2 - (\gamma-1)q^2(1-z) \\ 2(\gamma-1)u(1-z) \\ 2(\gamma-1)v(1-z) \\ 2(\gamma-1)(z-1) \\ 2(\gamma-1)q_0(1-z) - 2c^2 \end{pmatrix}, \quad \mathbf{l}_4^T = \frac{1}{2c^2}\begin{pmatrix} -\hat{v}c - (\gamma-1)z\frac{q^2}{2} \\ k_2 c + (\gamma-1)uz \\ -k_1 c + (\gamma-1)vz \\ -(\gamma-1)z \\ c^2 + (\gamma-1)q_0 z \end{pmatrix}$$

$$\mathbf{l}_5^T = \frac{1}{2c^2}\begin{pmatrix} -\hat{u}c + (\gamma-1)\frac{q^2}{2} \\ k_1 c - (\gamma-1)u \\ k_2 c - (\gamma-1)v \\ \gamma - 1 \\ -(\gamma-1)q_0 \end{pmatrix}, \quad \hat{v} = k_2 u - k_1 v$$

The matrix with the **l**:s as rows is the inverse of the matrix with **r**:s as columns.

In the exact (Godunov) Riemann solver, we first solve the Riemann problem for the non reactive Euler equations. The additional equation

$$(\rho z)_t + (u\rho z)_x = 0$$

is incorporated by choosing $\rho z = (\rho z)_L$ to the left of the contact discontinuity and $\rho z = (\rho z)_R$ to the right. The situation analogous to the two dimensional non reactive Euler equations, where the tangential velocity component v is convected along the u characteristics.